PCCP
Physical Chemistry Chemical Physics

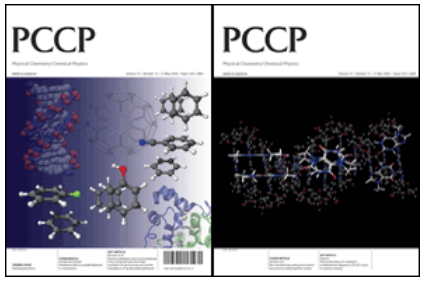

This paper is published as part of a PCCP Themed Issue on:

Stacking Interactions

Guest Editor: Pavel Hobza

Editorial

Perspectives

Papers

Structures and interaction energies of stacked graphene–nucleobase complexes
Jens Antony and Stefan Grimme, *Phys. Chem. Chem. Phys.*, 2008, **10**, 2722

Describing weak interactions of biomolecules with dispersion-corrected density functional theory
I-Chun Lin and Ursula Rothlisberger, *Phys. Chem. Chem. Phys.*, 2008, **10**, 2730

Physical origins of interactions in dimers of polycyclic aromatic hydrocarbons
Rafał Podeszwa and Krzysztof Szalewicz, *Phys. Chem. Chem. Phys.*, 2008, **10**, 2735

Benchmark database on isolated small peptides containing an aromatic side chain: comparison between wave function and density functional theory methods and empirical force field
Haydee Valdes, Kristýna Pluháčková, Michal Pitonák, Jan Řezáč and Pavel Hobza, *Phys. Chem. Chem. Phys.*, 2008, **10**, 2747

Scope and limitations of the SCS-MP2 method for stacking and hydrogen bonding interactions
Rafał A. Bachorz, Florian A. Bischoff, Sebastian Höfener, Wim Klopper, Philipp Ottiger, Roman Leist, Jann A. Frey and Samuel Leutwyler, *Phys. Chem. Chem. Phys.*, 2008, **10**, 2758

The interaction of carbohydrates and amino acids with aromatic systems studied by density functional and semi-empirical molecular orbital calculations with dispersion corrections
Raman Sharma, Jonathan P. McNamara, Rajesh K. Raju, Mark A. Vincent, Ian H. Hillier and Claudio A. Morgado, *Phys. Chem. Chem. Phys.*, 2008, **10**, 2767

Probing the effects of heterogeneity on delocalized π···π interaction energies
Desiree M. Bates, Julie A. Anderson, Ponmile Oloyede and Gregory S. Tschumper, *Phys. Chem. Chem. Phys.*, 2008, **10**, 2775

Competition between stacking and hydrogen bonding: theoretical study of the phenol···Ar cation and neutral complex and comparison to experiment
Jiří Černý, Xin Tong, Pavel Hobza and Klaus Müller-Dethlefs, *Phys. Chem. Chem. Phys.*, 2008, **10**, 2780

Calculating stacking interactions in nucleic acid base-pair steps using spin-component scaling and local second order Møller–Plesset perturbation theory
J. Grant Hill and James A. Platts, *Phys. Chem. Chem. Phys.*, 2008, **10**, 2785

Controlled aggregation of adenine by sugars: physicochemical studies, molecular modelling simulations of sugar–aromatic CH–π stacking interactions, and biological significance
Marc Maresca, Adel Derghal, Céline Carravagna, Séverine Dudin and Jacques Fantini, *Phys. Chem. Chem. Phys.*, 2008, **10**, 2792

Computational comparison of the stacking interactions between the aromatic amino acids and the natural or (cationic) methylated nucleobases
Lesley R. Rutledge, Holly F. Durst and Stacey D. Wetmore, *Phys. Chem. Chem. Phys.*, 2008, **10**, 2801

Computational characterization and modeling of buckyball tweezers: density functional study of concave–convex π···π interactions
Yan Zhao and Donald G. Truhlar, *Phys. Chem. Chem. Phys.*, 2008, **10**, 2813

Non-standard base pairing and stacked structures in methyl xanthine clusters
Michael P. Callahan, Zsolt Gengeliczki, Nathan Svadlenak, Haydee Valdes, Pavel Hobza and Mattanjah S. de Vries, *Phys. Chem. Chem. Phys.*, 2008, **10**, 2819

N–H···π interactions in pyrroles: systematic trends from the vibrational spectroscopy of clusters
Ingo Dauster, Corey A. Rice, Philipp Zielke and Martin A. Suhm, *Phys. Chem. Chem. Phys.*, 2008, **10**, 2827

Experimental and theoretical determination of the accurate interaction energies in benzene–halomethane: the unique nature of the activated CH/π interaction of haloalkanes
Asuka Fujii, Kenta Shibasaki, Takaki Kazama, Ryousuke Itaya, Naohiko Mikami and Seiji Tsuzuki, *Phys. Chem. Chem. Phys.*, 2008, **10**, 2836

IR/UV spectra and quantum chemical calculations of Trp–Ser: Stacking interactions between backbone and indole side-chain
Thomas Häber, Kai Seefeld, Gernot Engler, Stefan Grimme and Karl Kleinermanns, *Phys. Chem. Chem. Phys.*, 2008, **10**, 2844

Fluorine substitution and nonconventional OH···π intramolecular bond: high-resolution UV spectroscopy and *ab initio* calculations of 2-(*p*-fluorophenyl)ethanol
Rosen Karaminkov, Sotir Chervenkov and Hans J. Neusser, *Phys. Chem. Chem. Phys.*, 2008, **10**, 2852

CH/π interactions in methane clusters with polycyclic aromatic hydrocarbons
Seiji Tsuzuki, Kazumasa Honda, Asuka Fujii, Tadafumi Uchimaru and Masuhiro Mikami, *Phys. Chem. Chem. Phys.*, 2008, **10**, 2860

PCCP

Physical Chemistry Chemical Physics

www.rsc.org/pccp

Volume 10 | Number 19 | 21 May 2008 | Pages 2561–2868

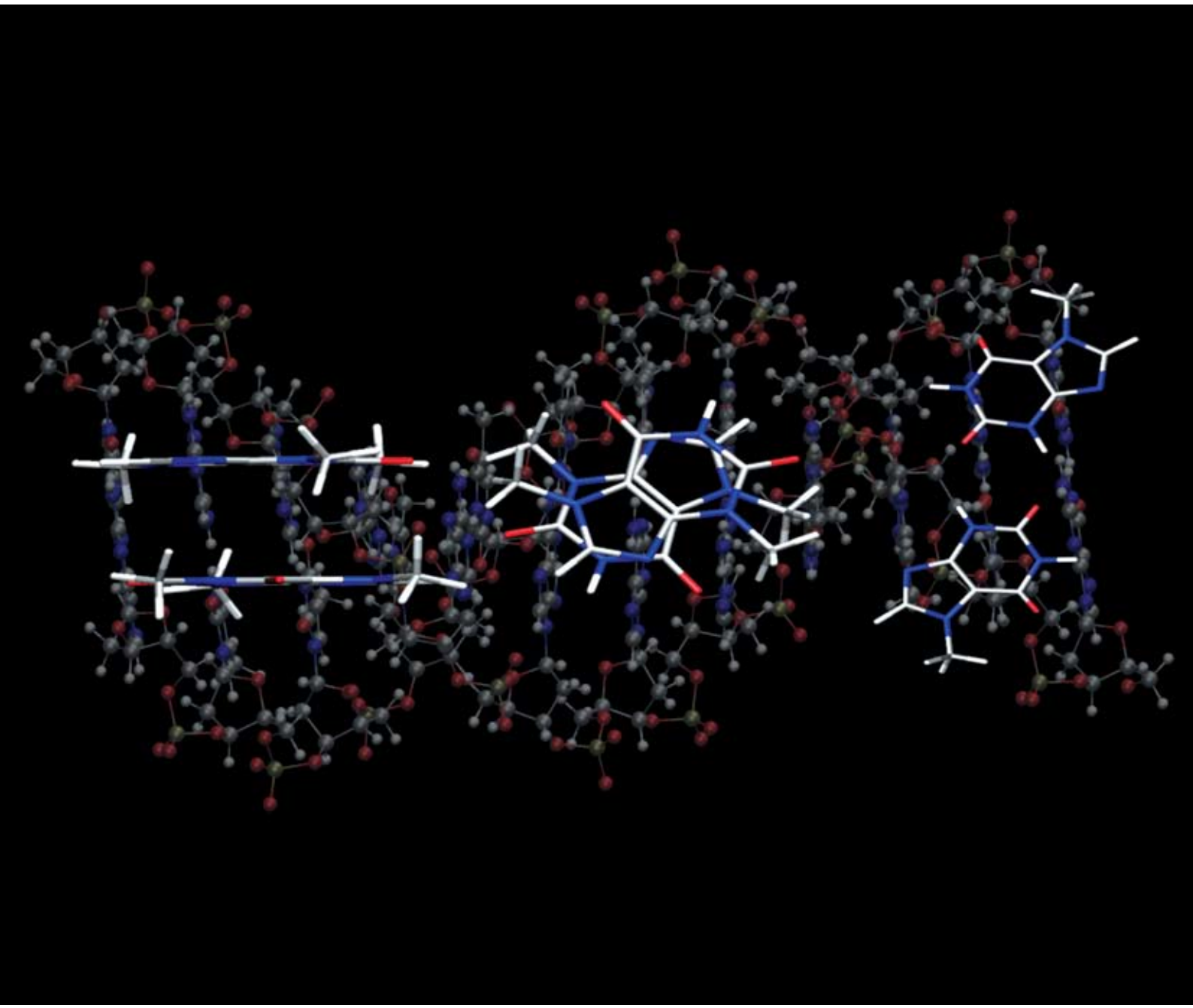

ISSN 1463-9076

COVER ARTICLE
de Vries *et al.*
Non-standard base pairing and stacked structures in methyl xanthine clusters

HOT ARTICLE
Improta
The excited states of π-stacked 9-methyladenine oligomers: a TD-DFT study in aqueous solution

Non-standard base pairing and stacked structures in methyl xanthine clusters†

Michael P. Callahan,[a] Zsolt Gengeliczki,[b] Nathan Svadlenak,[a] Haydee Valdes,[c] Pavel Hobza[c] and Mattanjah S. de Vries*[a]

Received 2nd January 2008, Accepted 4th February 2008
First published as an Advance Article on the web 17th March 2008
DOI: 10.1039/b719874d

We present resonant two-photon ionization and IR–UV double resonance spectra of methylated xanthine derivatives including 7-methylxanthine dimer and theobromine dimer seeded in a supersonic jet by laser desorption. For 7-methylxanthine, theophylline and theobromine monomer we assign the lowest energy tautomer based on comparison with IR–UV double resonance spectra and calculated IR frequencies. For the 7-methylxanthine dimer, we observe hydrogen bonding on the N3H position suggesting 3 possible combinations, one that is reverse Watson–Crick type and two that are reverse Hoogsteen type. For the theobromine dimer, we observe a stacked structure. For trimethylxanthine dimers we infer a stacked structure as well.

1. Introduction

Both hydrogen bonding and π–π interactions (or stacking interactions) play an important role in biological structures. Hydrogen bonding is responsible for base pair recognition in DNA and stabilizes α-helices and β-sheets in protein structures. Stacking interactions help stabilize the structure of DNA duplexes.[1] Gas-phase laser spectroscopy provides a means to study the intrinsic properties of biologically relevant molecules in a solvent-free environment, allowing detailed studies of the non-covalent forces that govern their interactions. Pairings of various nucleobases by hydrogen bonding have been extensively studied by these techniques,[2–8] however, only a few studies exist of stacked structures.

Theoretical calculations show that in the gas phase, hydrogen-bonded structures between nucleobases dominate.[9] The population of stacked structures can be enhanced in one of two ways. First, water molecules can stabilize stacked structures by bridging.[9–11] Kabeláč *et al.* predict that two to six water molecules are required for most nucleobases' pair combinations to cause stacked structures to be preferred over H-bonded ones.[9] Second, methylation can lead to stacking by reducing the number of H-bonding sites. Kabeláč *et al.* have shown that 7-methyladenine–adenine adopts a nearly planar hydrogen bonded structure and 9-methyladenine-adenine adopts a stacked structure.[12] Here we further explore this aspect of competition between stacking and H-bonding by studying clusters of various methylated xanthines. Fig. 1 shows the methyl derivatives used in this work.

Methyl xanthines are important molecules commonly used as mild stimulants and bronchodilators.[13] In the gas phase, these purines can exist in a variety of different tautomeric forms, which can exhibit drastically different photophysical behavior. We investigated the structure of 7-methylxanthine dimer and theobromine dimer by resonant two-photon ionization (R2PI) and IR–UV double resonance spectroscopy. By comparing the observed IR–UV spectra with calculated frequencies of optimized structures, we conclude that 7-methylxanthine dimer is most likely hydrogen bonded in the three-position and theobromine dimer is in a stacked configuration.

2. Methods

Experimental

7-Methylxanthine, theophylline (1,3-dimethylxanthine), theobromine (3,7-dimethylxanthine), and caffeine (1,3,7-trimethylxanthine) were obtained from Sigma-Aldrich and used without further purification.

The experimental setup has been described in detail elsewhere.[14] We laser desorb a thin layer of sample from a graphite substrate in front of a pulsed nozzle. The desorption laser, an Nd:YAG operating at 1064 nm, is attenuated to 1 mJ cm^{-2} and focused to a spot of approximately 0.5 mm diameter within 2 mm in front of the nozzle orifice. We translate the sample in order to expose fresh sample to successive laser shots. The nozzle consists of a pulsed valve with a nozzle diameter of

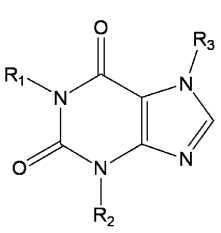

	R_1	R_2	R_3
7-methylxanthine	H	H	CH_3
theobromine	H	CH_3	CH_3
theophylline	CH_3	CH_3	H
caffeine	CH_3	CH_3	CH_3

Fig. 1 The structures of methyl xanthine derivatives examined in this report.

[a] *Department of Chemistry and Biochemistry, University of California, Santa Barbara, CA 93106-9510, USA*
[b] *Institute of Chemistry, Eötvös Loránd University, 1/A Pázmány P. stny. Budapest, 1117, Hungary*
[c] *Center for Biomolecules and Complex Molecular Systems, Institute of Organic Chemistry and Biochemistry, Academy of Sciences of the Czech Republic, 116 10 Prague 6, Czech Republic*

† Electronic supplementary information (ESI) available: IR–UV double resonance spectra. See DOI: 10.1039/b719874d

1 mm and a backing pressure of 6 atm of argon drive gas. The neutral molecules are skimmed and then ionized with a frequency-doubled dye laser. We detect the ions in a reflectron time-of-flight mass spectrometer. Typical mass resolution ($m/\Delta m$) measured at the molecular ion peak is 700 or higher.

We obtain resonant two-photon ionization (R2PI) spectra by monitoring mass selected peaks while tuning the one-color, two-photon ionization (1C-R2PI) wavelength. For theobromine and caffeine, we also ionized these molecules using a two-color two-photon process (2C-R2PI). For the second photon we used 266 nm provided by the fourth harmonic of another Nd:YAG laser. We measure IR–UV double resonance spectra with two laser pulses separated in time by 200 ns. The first IR pulse serves as a "burn" pulse, which removes the ground state population and causes depletion in the ion signal of the second UV "probe" pulse, provided both lasers are tuned to a resonance of the same isomer. IR frequencies are produced in an OPO/OPA setup (LaserVision) pumped by a Nd:YAG laser operating at its fundamental frequency. For this work, we operated within the range of 2800–3550 cm^{-1}, which encompasses NH and OH modes. Typical IR intensities in the burn region are 12 mJ $pulse^{-1}$ and the bandwidth is 3 cm^{-1}.

Theoretical

We assessed the tautomeric equilibria of methylated xanthines using the Gaussian 03 quantum code package.[15] Application of density functional theory's B3LYP hybrid functional (a parameterized combination of Becke's exchange functional, the Lee, Yang and Parr correlation functional and the exact exchange functional)[16–18] with a 6-311 + G(2d,p) basis set[19,20] yielded equilibrium geometries of the tautomers for each methylated xanthine. We performed second derivative calculations for purposes of vibrational frequency analysis and to verify that the geometries for all species corresponded to local minima. Vibrational frequencies were computed on an ultrafine grid and a corrective scaling factor of 0.9618 was applied to account for anharmonicity.[21]

We used the MD/Q technique, described elsewhere,[22] to scan the potential-energy surface (PES) of the theobromine and caffeine dimers, employing the self-consistent charge density functional tight-binding method extended by an empirical dispersion term (SCC-DF-TB-D).[23] The most stable structures according to the SCC-DF-TB-D level of theory were selected (they were contained within an interval of energy of 9 kcal/mol) and reoptimized using the RI-DFT-D[24] method in combination with the TPSS[25] functional augmented with dispersion energy (TPSS-D) and the 6-311 + + G(3df,3dp)[26] basis set. The RI-DFT-D method is home implemented in the Turbomole 5.9 program package.[27] Vibrational frequencies were calculated at the same level of theory in the context of the rigid rotor, harmonic oscillator, ideal gas approximation. A corrective scaling factor of 0.988 was applied.

3. Results and discussion

3.1 Methyl xanthine monomers

We measured one-color R2PI spectra for 7-methylxanthine and theophylline, and two-color R2PI spectra for theobromine and caffeine, shown in Fig. 2. One-color R2PI was possible for both theobromine and caffeine, but peaks were broadened due to power saturation, which led to increased spectral congestion. By performing two-color R2PI, separating excitation and ionization, we could reduce the intensity of the excitation laser. This approach reduced power broadening and produced better spectra. The R2PI spectra for all of these methylated xanthines are sharp and vibronically resolved. Increasing the number of methyl substitutions on xanthine shifts the R2PI spectra to lower energies. To identify specific tautomers in this R2PI region, we measured IR–UV double resonance spectra on the origin peak for 7-methylxanthine, theophylline, and theobromine. For all three monomers, we observe the lowest energy tautomer based on the following analysis of our IR–UV spectra.

Fig. 3 shows the IR–UV double resonance spectrum of 7-methylxanthine along with the calculated frequencies for five tautomers optimized at the B3LYP/6-311 + G(2d,p) level. By comparing the IR–UV spectrum to the calculated frequencies and intensities, we conclude that we observe the diketo 7-methylxanthine which we calculated to be the lowest energy tautomer. The two strong bands at 3445 and 3485 cm^{-1} in the IR–UV spectrum can be assigned as the N1H and N3H

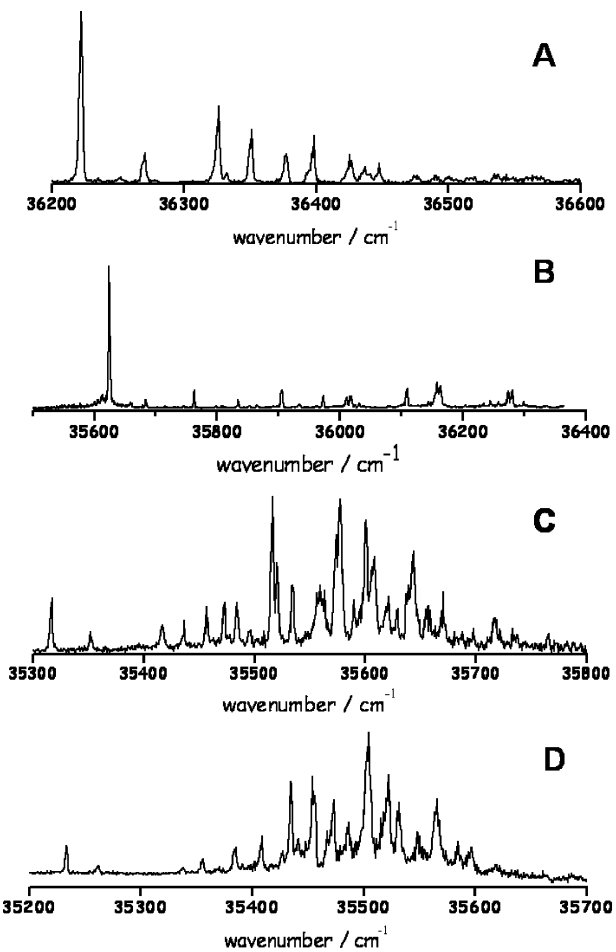

Fig. 2 The R2PI spectra of (A) 7-methylxanthine, (B) theophylline, (C) theobromine, and (D) caffeine. The theobromine and caffeine spectra are two-color R2PI with 266 nm.

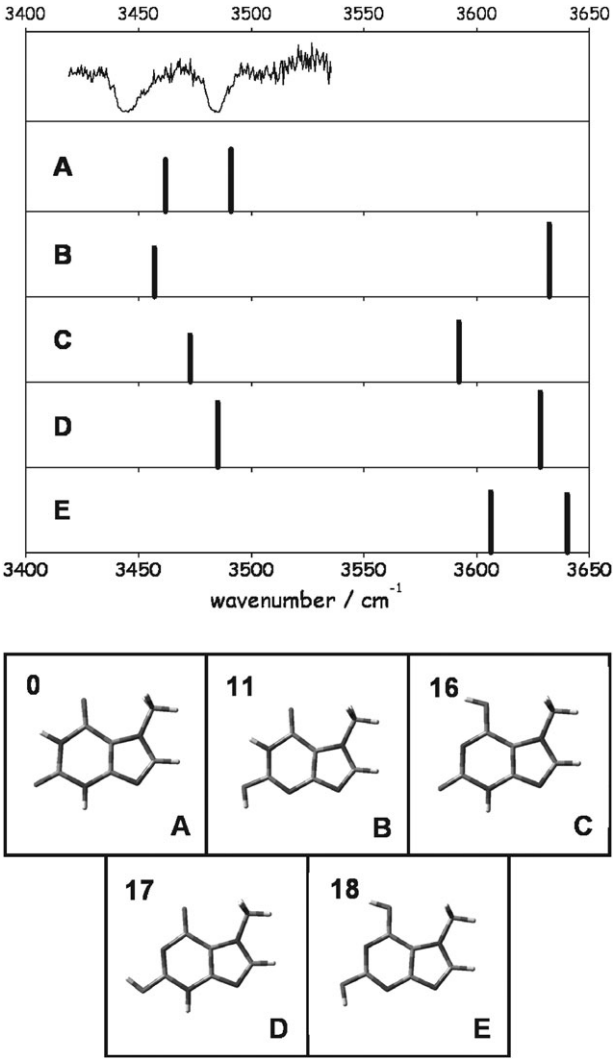

Fig. 3 IR–UV double resonance spectrum of 7-methylxanthine. Stick spectra are calculated frequencies at the B3LYP/6-311 + G(2d,p) level for tautomers of 7-methylxanthine (lettered A–E). Their relative energies (in kcal/mol) are shown in the upper left hand corner.

stretching vibrations. The other four tautomers are higher in energy by at least 11 kcal/mol and their calculated IR frequencies do not match the experimental result.

Fig. 4 shows the IR–UV double resonance spectrum of theophylline along with the calculated frequencies for three tautomers optimized at the B3LYP/6-311 + G(2d,p) level. The lowest energy tautomer is the N7H form, while the N9H tautomer is 9 kcal/mol higher in energy. However, the calculated N–H stretching vibrations for these two tautomers are almost indistinguishable from each other. In another report, we measured the IR–UV double resonance spectrum of xanthine and assigned it to the N7H form.[28] In xanthine, the differences in the calculated frequencies between the N7H and N9H forms were larger despite similar energy differences. By comparison of IR–UV spectra, it would seem that theophylline is also in the N7H form (see ESI).† Therefore, we tentatively assign the one band at 3500 cm^{-1} in the IR–UV spectrum as the N7H stretching vibration. The third tautomer is an unlikely assignment since it is much higher in energy

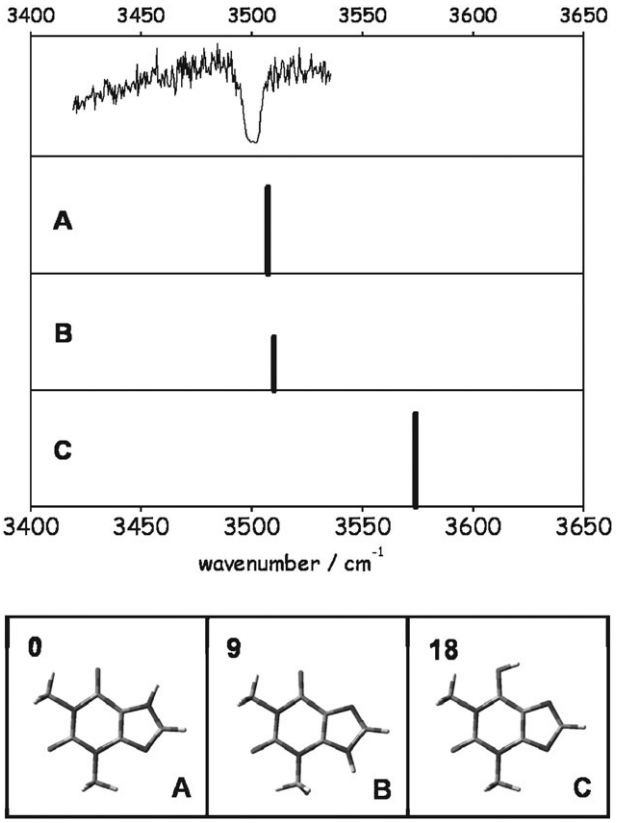

Fig. 4 IR–UV double resonance spectrum of theophylline. Stick spectra are calculated frequencies at the B3LYP/6-311 + G(2d,p) level for tautomers of theophylline (lettered A–C). Their relative energies (in kcal/mol) are shown in the upper left hand corner.

(18 kcal/mol) in addition to the poorer match for the IR frequency.

Fig. 5 shows the IR–UV double resonance spectrum of theobromine along with the calculated frequencies for three tautomers optimized at the B3LYP/6-311 + G(2d,p) level. By comparing the IR–UV spectrum to the calculated frequencies and intensities, we conclude that we observe the diketo form in the supersonic jet. This is the most confident assignment since the other two tautomers are much higher in energy (greater than 16 kcal/mol). In addition, the calculated OH band for the enol forms is more than 100 cm^{-1} away from the one band in the experimental IR–UV spectrum at 3446 cm^{-1}, assigned as the N1H stretching vibration. For caffeine, we did not measure the IR–UV double resonance spectrum since all three N–H sites are replaced by methyl groups.

3.2 7-Methylxanthine dimer

Fig. 6 shows the one-color R2PI spectrum for 7-methylxanthine dimer. Its appearance differs significantly from that of the 7-methylxanthine monomer. The R2PI spectrum is red-shifted compared to the monomer and broad. Fig. 7 shows a mass spectrum recorded at 35 677 cm^{-1} exhibiting a strong peak for the 7-methylxanthine dimer. A very small peak for the 7-methylxanthine trimer was the only other peak observed in the mass spectrum. Despite optimization on the dimer peak, we cannot exclude the possibility that the dimer spectrum contains

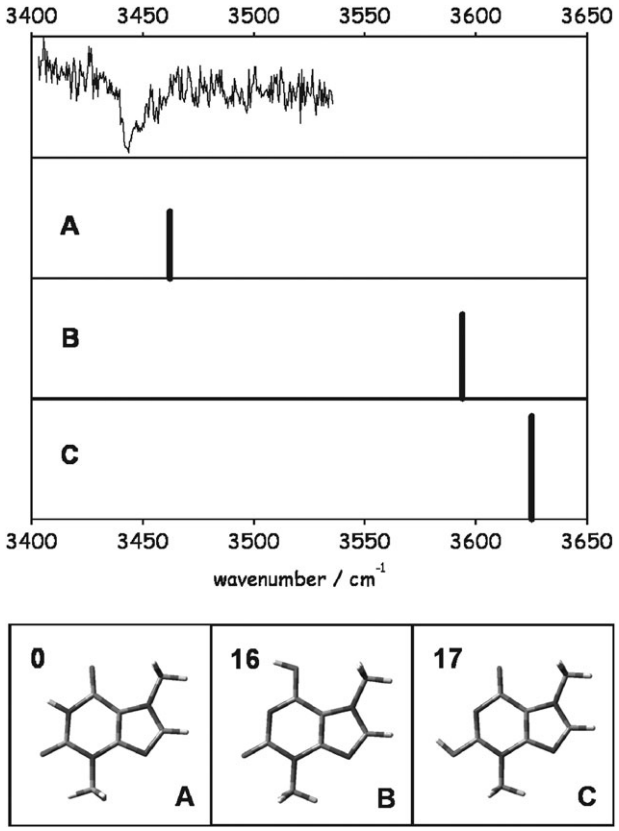

Fig. 5 IR–UV double resonance spectrum of theobromine. Stick spectra are calculated frequencies at the B3LYP/6-311 + G(2d,p) level for tautomers of theobromine (lettered A–C). Their relative energies (in kcal/mol) are shown in the upper left hand corner.

contributions from higher clusters fragmenting. However, we are confident that the R2PI spectrum for 7-methylxanthine monomer does not contain contributions from the dimer because they absorb in different spectral regions.

We calculated energies and IR frequencies for the 7-methylxanthine dimer at the B3LYP/6-311 + G(2d,p) level. We did this for 10 different combinations where both molecules are in the lowest energy diketo form. These base pairs are all close in energy, where the lowest and highest energy combinations are only separated by 3 kcal/mol, as summarized in Fig. 8. Other combinations were not considered since enol and dienol

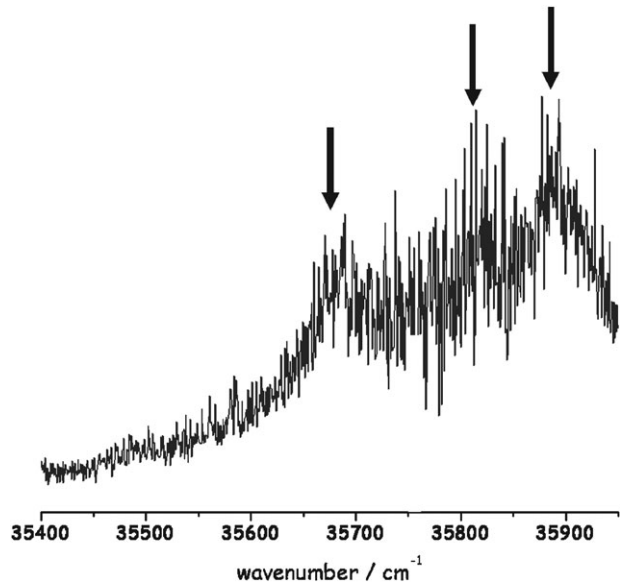

Fig. 6 The broad, one-color R2PI spectrum of 7-methylxanthine dimer. The arrows at 35 677, 35 822 and 35 892 cm^{-1} indicate where IR spectra were measured by double resonant techniques.

tautomers are much higher in energy and their presence is unlikely in the supersonic expansion. The IR–UV double resonance spectrum for the 7-methylxanthine monomer shows two strong bands at 3445 and 3485 cm^{-1}, which correspond to the computed N1H and N3H stretch frequencies. We measured the IR–UV double resonance spectrum for the 7-methylxanthine dimer while probing at three different UV frequencies: 35 677, 35 822 and 35 892 cm^{-1}. The IR–UV spectra probed at each UV frequency were essentially identical. In these spectra, shown in Fig. 9, the N3H band is absent, which indicates that this position is now involved in a hydrogen bond. In addition, two strong broad bands are observed below 3200 cm^{-1}, with one especially broad band spanning from 3130 to 2875 cm^{-1}. Attenuating the IR output in this broad region did not change the appearance of the IR–UV spectrum.

Of the 10 calculated dimer structures, the three lowest energy base pairs are the only ones where the N3H in both molecules are involved in hydrogen bonds. The lowest energy

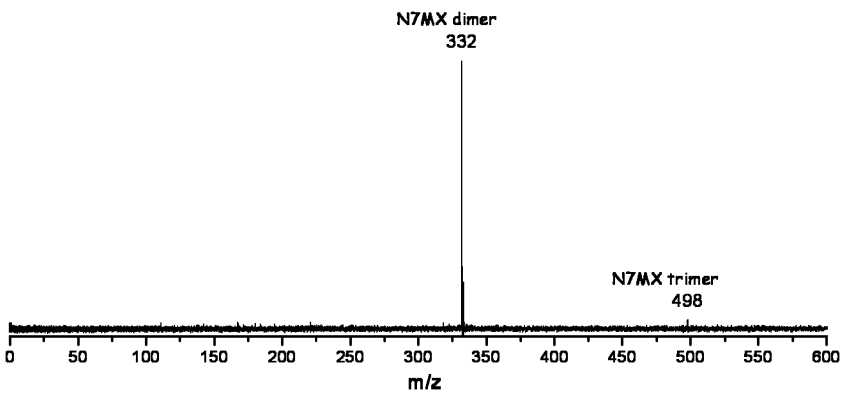

Fig. 7 Mass spectrum recorded at 35 677 cm^{-1} showing a strong 7-methylxanthine dimer peak.

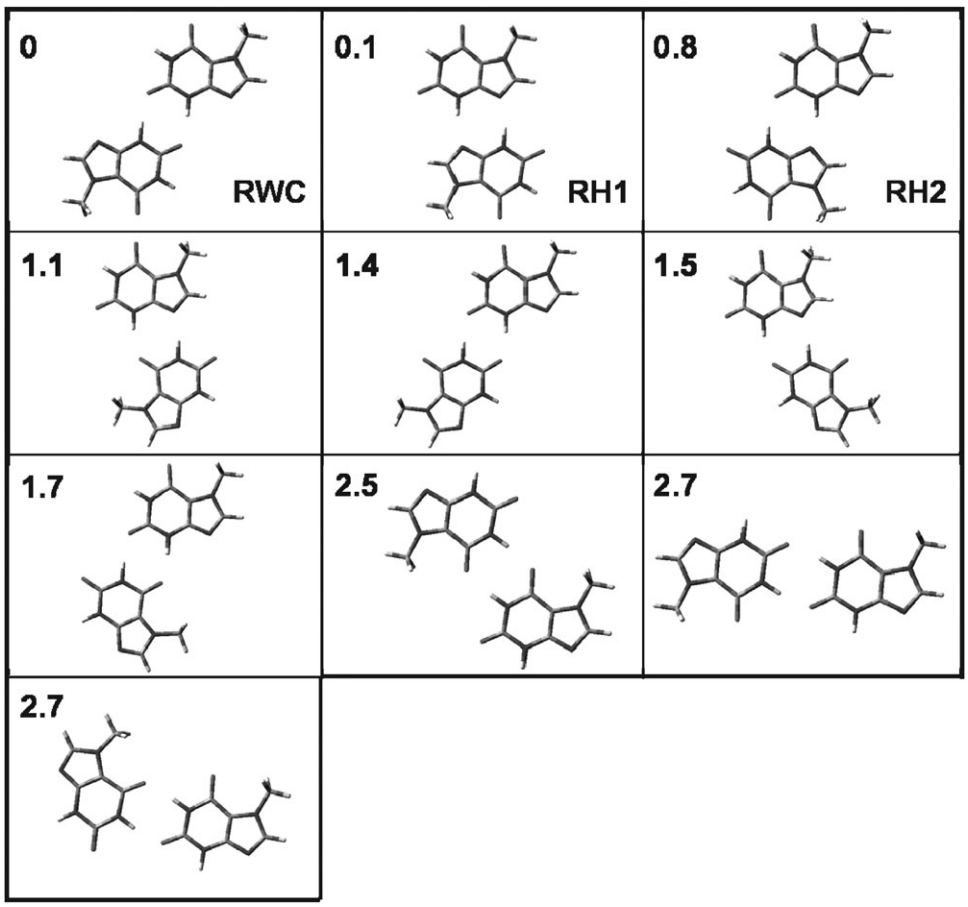

Fig. 8 The relative energies (in kcal/mol) of the 7-methylxanthine dimer calculated at the B3LYP/6-311 + G(2d,p) level. The three lowest energy base pairs all have their N3H involved in hydrogen bonding. One base pair is reverse Watson–Crick (RWC) and the other two are reverse Hoogsteen (RH1 and RH2).

pair is in a reverse Watson–Crick (RWC) type configuration and the other two pairs are in reverse Hoogsteen (RH1 and RH2) type configurations. The calculated IR frequencies for the N1H stretching vibration in these configurations are in the same position and fit the experimental band well.

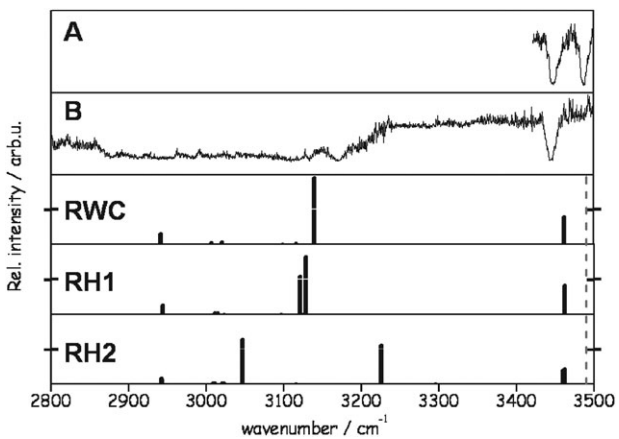

Fig. 9 IR–UV double resonance spectrum of (A) 7-methylxanthine monomer and (B) 7-methylxanthine dimer. Stick spectra are calculated frequencies at the B3LYP/6-311 + G(2d,p) level for the three lowest energy dimer structures. In all three dimer structures, the N1H is free. The dotted red line is the calculated N3H stretch, which matches the IR band in the monomer spectrum very well.

However, establishing the exact base pair configuration observed in our experiment is difficult due to the broad nature of the IR bands below 3200 cm^{-1}. For the reverse Watson–Crick (RWC) base pair we calculated one strong IR band at 3140 cm^{-1}, which corresponds to N3Hs hydrogen bonded to oxygen atoms at the two-position. For the lower energy reverse Hoogsteen base pair (RH1), we calculated two strong IR bands around 3121 and 3128 cm^{-1}, which correspond to N3Hs hydrogen bonded to nitrogen atoms at the nine-position. For the higher energy reverse Hoogsteen base pair (RH2), we calculated two strong IR bands around 3047 and 3226 cm^{-1}, which correspond to the N3H hydrogen bonded to the nitrogen atom at the nine-position and the other N3H hydrogen bonded to oxygen atoms at the two-position respectively. The latter calculated band is a good fit to the experimental band at 3170 cm^{-1}. The extremely broad bands in the experimental IR–UV spectrum could be explained by the overlap of frequencies from all three dimer structures. In addition, the broad and congested R2PI spectrum can be the result of overlapping spectra from multiple similar structures. Furthermore, photophysics similar to that found in various nucleobases might also contribute to spectral broadening in the UV.

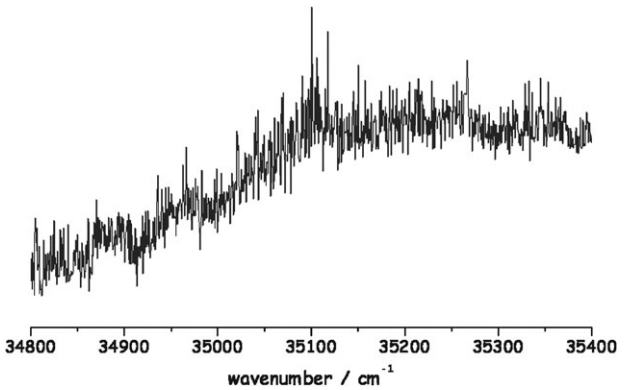

Fig. 10 The broad, one-color R2PI spectrum of theobromine dimer.

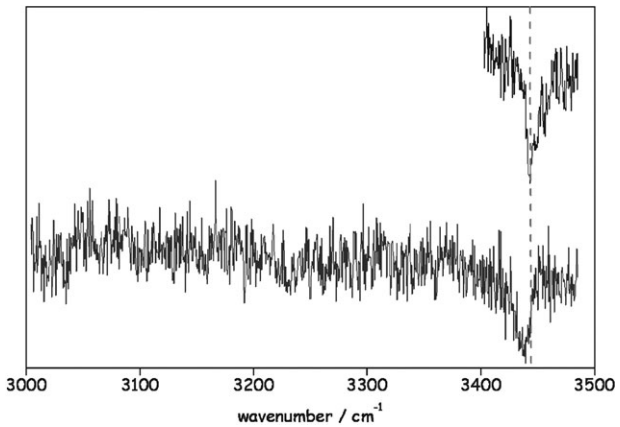

Fig. 11 IR–UV double resonance spectra of theobromine monomer (top trace) and theobromine dimer (bottom trace). The IR band for the dimer is slightly red-shifted with respect to the IR band for the monomer.

There is also a possibility for different tautomeric structures in which three hydrogen bonds are formed either by two enol tautomers or one diketo and one dienol tautomer. This could occur if the stabilization of the three hydrogen bonds would be greater than the reorganization energy of the tautomers. However all of these combinations have a free N3H mode and therefore do not fit the experimental IR–UV data. In addition, Dietrich *et al*. have calculated that these base pairs containing three hydrogen bonds are much less stable compared to those with two hydrogen bonds involving the N3H position.[29]

3.3 Theobromine dimer

Fig. 10 shows the one-color R2PI spectrum for theobromine dimer. Again, the R2PI spectrum of the dimer is broad compared to the sharp and resolved R2PI spectrum of the monomer. The onset of the R2PI spectrum for theobromine dimer is red-shifted compared to the monomer.

Fig. 11 shows the IR–UV double resonance spectra for the theobromine monomer and dimer. Both the monomer and dimer feature a strong band, around 3446 and 3438 cm^{-1} respectively. Despite a slight shift of the IR band observed in the dimer, they clearly fit the N1H stretch frequency. The experimental IR–UV spectrum indicates that the dimer structure is in a stacked configuration rather than hydrogen bonded one. A stacked structure for theobromine dimer may partly explain the broad appearance of the R2PI spectrum, since mixing of electronic states is more likely to occur. Broad excitation spectra are commonly observed for aromatic dimers due to stacking interactions and excimer formation.[30,31]

Fig. 12 shows the structures and relative energies (in kcal/mol) of the theobromine dimer optimized at the RI-DFT-D/TPSS-D/6-311++G(3df,3dp) level. All calculated frequencies for the theobromine dimer are shown in Table 1. Eleven of the fourteen calculated structures are in a stacked configuration. The remaining three structures are hydrogen bonded and can be ruled out as possibilities based on their calculated frequencies. While these data clearly indicate stacking, it is difficult to assign a specific stacked structure to fit the IR–UV double resonance spectrum. We observed only one IR band (at 3438 cm^{-1}) for theobromine dimer, which we can use to compare with theoretically calculated frequencies. However, calculated

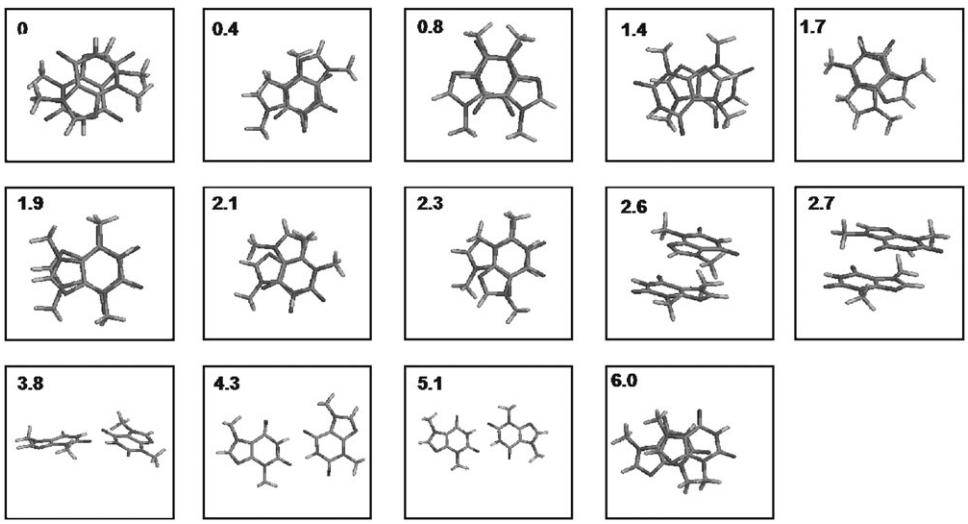

Fig. 12 The structures and relative energies (in kcal/mol) of the theobromine dimer optimized at the RI-DFT-D/TPSS-D/6-311++G(3df,3dp) level.

Table 1 Theoretical (RI-DFT-D/TPSS/6-311++G(3df,3pd)) vibrational frequencies (in cm^{-1}) for the most stable conformers in the FES of theobromine dimer. A scaling factor of 0.988 has been applied

	$NH_{H\text{-bonded}}$	NH_{free}	NH_{free}
str_01	—	3500	3499
str_02	—	3489[a]	3489[a]
str_03	—	3499	3498
str_04	—	3499	3498
str_05	—	3483[a]	3481[a]
str_06	—	3485	3484
str_07	—	3488	3482
str_08	—	3484[a]	3483[a]
str_09	—	3499	3495
str_10	—	3500	3496
str_11	3092	—	—
str_12	3116	—	—
str_13	3055	—	—
str_14	—	3498	3480

[a] Neighboring vibration modes are coupled.

frequencies for the N1H modes all appear in the same region around 3500 cm^{-1}. In addition, the calculated frequencies for the individual N1H modes are spaced very closely together in most of the stacked configurations. Hence, these would likely appear as one peak in our experimental spectrum (since we are limited by the bandwidth of our IR OPO/OPA). This situation would apply to seven out of the eleven calculated stacked structures. These seven stacked structures are all close in energy (within 6 kcal/mol) and could all be present in the supersonic jet. Therefore, we can only conclude that we observe a stacked structure along with the possibility that we may be observing multiple configurations.

3.4 Caffeine and theophylline dimers

For caffeine, we observe a very strong dimer signal in the mass spectrum. Since all hydrogen bonding sites are blocked we did not measure an IR–UV spectrum and these must be van der Waals dimers based on π-stacking. For caffeine dimer, we ran molecular dynamics simulations at various temperatures ranging from 100 K to 1100 K, obtaining different stacked geometries of which Fig. 13 shows an example. Further computation is needed for an accurate prediction of its structure.

Curiously, we do not observe any theophylline dimer despite the fact we can observe caffeine dimers, which one would expect to exhibit more steric hindrance for dimer formation. We note that cluster formation, in principle, occurs readily in our experiment because by adjusting the sample position relative to the pulsed nozzle, we can observe theophylline–argon clusters in the mass spectrum. It is possible for species to be present in the molecular beam without being observed by R2PI detection. Possible reasons include unfavorable Franck–Condon factors, spectral shifts, low oscillator strengths, or short excited state lifetimes compared to the nanosecond timescale laser pulses. These effects could also play a role in the failure to observe hydrogen bonded theobromine dimers and all but the three lowest energy structures of 7-methylxanthine dimer. Since for the latter the calculated energy differences are very small this would suggest structure-dependent photochemistry.

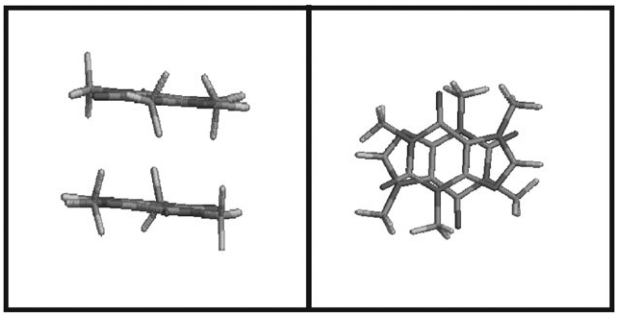

Fig. 13 Stacked structure of caffeine dimer based on a molecular dynamics simulation.

4. Conclusion

We investigated the gas-phase structure of various methylated xanthine derivatives including 7-methylxanthine dimer and theobromine dimer by resonant two-photon ionization and IR–UV double resonance spectroscopy. The R2PI spectra for 7-methylxanthine, theophylline, theobromine, and caffeine were sharp and vibronically resolved. Based on calculated frequencies, we assigned the IR–UV spectra for these monomers to their lowest energy tautomer in each case. The R2PI spectra for 7-methylxanthine dimer and theobromine dimer are red-shifted and broad compared to their respective monomers. By comparing the observed IR–UV spectra with calculated frequencies for optimized dimer structures, we conclude that the 7-methylxanthine dimer is hydrogen bonded on the N3H position suggesting 3 possible combinations: one that is of a reverse Watson–Crick type and two that are reverse Hoogsteen type structures. We assign a stacked structure to theobromine dimer since its IR–UV spectrum is similar to that of theobromine monomer with a free NH group and suggesting absence of hydrogen bonding. Hydrogen bonding would still be possible in this dimer, so it appears that increasing the number of methylated sites does increase the probability of stacking interactions in competition with hydrogen bonding.

Acknowledgements

This material is based upon work supported by the National Science Foundation under Grant No. CHE-0615401. Zsolt Gengeliczki gratefully acknowledges the generous support of the Rosztoczy Foundation. This study was partially supported by Grant LC512 from the Ministry of Education, Youth and Sports of the Czech Republic and it was also part of the research project No. Z4 055 0506. The support of Praemium Academiae awarded to PH in 2007 is also acknowledged.

References

1 D. Voet and J. G. Voet, *Biochemistry*, John Wiley and Sons, Inc., New York, 2004.
2 A. Abo-Riziq, L. Grace, E. Nir, M. Kabelac, P. Hobza and M. S. de Vries, *Proc. Natl. Acad. Sci. U. S. A.*, 2005, **102**, 20–23.
3 E. Nir, I. Hunig, K. Kleinermanns and M. S. de Vries, *Phys. Chem. Chem. Phys.* , 2003, **5**, 4780–4785.
4 E. Nir, C. Janzen, P. Imhof, K. Kleinermanns and M. S. de Vries, *Phys. Chem. Chem. Phys.*, 2002, **4**, 732–739.
5 E. Nir, C. Janzen, P. Imhof, K. Kleinermanns and M. S. de Vries, *Phys. Chem. Chem. Phys.* , 2002, **4**, 740–750.

6 E. Nir, K. Kleinermanns and M. S. de Vries, *Nature*, 2000, **408**, 949–951.
7 C. Plutzer, I. Hunig and K. Kleinermanns, *Phys. Chem. Chem. Phys.* , 2003, **5**, 1158–1163.
8 C. Plutzer, I. Hunig, K. Kleinermanns, E. Nir and M. S. de Vries, *ChemPhysChem*, 2003, **4**, 838–842.
9 M. Kabelac and P. Hobza, *Chem.–Eur. J.*, 2001, **7**, 2067–2074.
10 M. Kabelac, F. Ryjacek and P. Hobza, *Phys. Chem. Chem. Phys.*, 2000, **2**, 4906–4909.
11 D. Sivanesan, I. Sumathi and W. J. Welsh, *Chem. Phys. Lett.*, 2003, **367**, 351–360.
12 M. Kabelac, C. Plutzer, K. Kleinermanns and P. Hobza, *Phys. Chem. Chem. Phys.*, 2004, **6**, 2781–2785.
13 D. T. Hurst, *An Introduction to the Chemistry and Biochemistry of Pyrimidines, Purines and Pteridines*, Wiley, New York, 1980.
14 G. Meijer, M. S. Devries, H. E. Hunziker and H. R. Wendt, *Appl. Phys. B: Photophys. Laser Chem.*, 1990, **51**, 395–403.
15 M. J. Frisch, G. W. Trucks, H. B. Schlegel, G. E. Scuseria, M. A. Robb, J. R. Cheeseman, J. A. Montgomery, Jr., T. Vreven, K. N. Kudin, J. C. Burant, J. M. Millam, S. S. Iyengar, J. Tomasi, V. Barone, B. Mennucci, M. Cossi, G. Scalmani, N. Rega, G. A. Petersson, H. Nakatsuji, M. Hada, M. Ehara, K. Toyota, R. Fukuda, J. Hasegawa, M. Ishida, T. Nakajima, Y. Honda, O. Kitao, H. Nakai, M. Klene, X. Li, J. E. Knox, H. P. Hratchian, J. B. Cross, V. Bakken, C. Adamo, J. Jaramillo, R. Gomperts, R. E. Stratmann, O. Yazyev, A. J. Austin, R. Cammi, C. Pomelli, J. Ochterski, P. Y. Ayala, K. Morokuma, G. A. Voth, P. Salvador, J. J. Dannenberg, V. G. Zakrzewski, S. Dapprich, A. D. Daniels, M. C. Strain, O. Farkas, D. K. Malick, A. D. Rabuck, K. Raghavachari, J. B. Foresman, J. V. Ortiz, Q. Cui, A. G. Baboul, S. Clifford, J. Cioslowski, B. B. Stefanov, G. Liu, A. Liashenko, P. Piskorz, I. Komaromi, R. L. Martin, D. J. Fox, T. Keith, M. A. Al-Laham, C. Y. Peng, A. Nanayakkara, M. Challacombe, P. M. W. Gill, B. G. Johnson, W. Chen, M. W. Wong, C. Gonzalez and J. A. Pople, *GAUSSIAN 03 (Revision C.02)*, Gaussian, Inc., Wallingford, CT, 2004.
16 A. D. Becke, *J. Chem. Phys.*, 1993, **98**, 5648.
17 C. Lee, W. Yang and R. G. Parr, *Phys. Rev. B*, 1988, **37**, 785.
18 B. Miehlich, A. Savin, H. Stoll and H. Preuss, *Chem. Phys. Lett.*, 1989, **157**, 200.
19 R. Krishnan, J. S. Binkley, R. Seeger and J. A. Pople, *J. Chem. Phys.*, 1980, **72**, 650–654.
20 A. D. McLean and G. S. Chandler, *J. Chem. Phys.*, 1980, **72**, 5639–5648.
21 M. P. Andersson and P. Uvdal, *J. Phys. Chem. A*, 2005, **109**, 2937–2941.
22 F. Ryjacek, O. Engkvist, J. Vacek, M. Kratochvil and P. Hobza, *J. Phys. Chem. A*, 2001, **105**, 1197–1202.
23 M. Elstner, P. Hobza, T. Frauenheim, S. Suhai and E. Kaxiras, *J. Chem. Phys.*, 2001, **114**, 5149–5155.
24 P. Jurecka, J. Cerny, P. Hobza and D. R. Salahub, *J. Comput. Chem.*, 2007, **28**, 555–569.
25 J. M. Tao, J. P. Perdew, V. N. Staroverov and G. E. Scuseria, *Phys. Rev. Lett.*, 2003, **91**.
26 W. J. Hehre, L. Radom, P. V. Schleyer and J. A. Pople, Ab initio *Molecular Orbital Theory*, Wiley-Interscience, New York, 1986.
27 R. Ahlrichs, M. Bar, M. Haser, H. Horn and C. Kolmel, *Chem. Phys. Lett.*, 1989, **162**, 165–169.
28 M. P. Callahan, B. Crews, A. Abo-Riziq, L. Grace, M. S. de Vries, Z. Gengeliczki, T. M. Holmes and G. A. Hill, *Phys. Chem. Chem. Phys.*, 2007, **9**, 4587–4591.
29 B. Dietrich, T. A. Hupp and B. Engels, *NIC Symposium*, Julich, Germany, 2001.
30 F. Piuzzi, I. Dimicoli, M. Mons, P. Millie, V. Brenner, Q. Zhao, B. Soep and A. Tramer, *Chem. Phys.*, 2002, **275**, 123–147.
31 H. Saigusa and E. C. Lim, *Acc. Chem. Res.*, 1996, **29**, 171–178.

